# A Structurally Altered D,L-Amino Acid TCRα Transmembrane Peptide Interacts with the TCRα and Inhibits T-Cell Activation *in Vitro* and in an Animal Model†

Francisco J. Quintana,‡,§ Doron Gerber,§,|| Itai Bloch,|| Irun R. Cohen,‡ and Yechiel Shai*,||

*Departments of Immunology and Biological Chemistry, The Weizmann Institute of Science, Rehovot, 76100 Israel*

*Received September 5, 2006; Revised Manuscript Received January 2, 2007*

ABSTRACT: Protein−protein interactions in the membrane are pivotal for the cellular response to receptor-sensed stimuli. Recently, it has been demonstrated that an all-D-amino acids analogue of the TCRα transmembrane peptide (CP) is recruited to the TCR complex and inhibits T-cell activation *in vitro* and *in vivo*, similarly to the wild-type CP peptide. Here we investigated the relative contributions of the secondary structure of CP compared to its side chains in the association of CP with the TCR. We disrupted the secondary structure of CP by replacing two positive residues, needed for the interaction of CP with the TCR complex, by their D-enantiomers (2D-CP). Structure disruption was demonstrated by CD and FTIR spectroscopy, and molecular dynamics simulation in a bilayer environment. *In vitro*, 2D-CP colocalized with the TCR (visualized with confocal microscopy), immunoprecipitated with TCR but not MHC I, and inhibited T-cell activation. The peptide was effective also *in vivo*: it inhibited adjuvant arthritis in rats and delayed type hypersensitivity in BALB/c mice. Moreover, 2D-CP manifested greater immunosuppressive activity than wild-type CP, both *in vivo* and *in vitro*, which can be attributed to the greater solubility and resistance to degradation of 2D-CP. In molecular terms, these findings suggest that, under certain conditions, protein−protein interactions within the membrane might be more dependent on side chain interactions than on a specific secondary structure. The new altered secondary structure probably determines how the Lys and the Arg are positioned with respect to each other, so they can interact with the TM domain of the receptor. In clinical terms, the increased solubility and resistance to degradation of D-stereoisomers might be exploited in the targeted inactivation of pathogenic signaling pathways such as those arising from TCR-triggered activation of T-cells in immune-mediated disorders.

Protein−protein interactions within the cell membrane are key events for the control of many biological responses. They are thought to be governed by the secondary structure of the transmembrane domains (TM) of the interacting proteins, predominantly α-helices, through the formation of different bonds between their side chains (*1*−*3*). Many studies were reported on helix−helix interaction within the membrane milieu via various motifs. These include: the GxxxG motif found in various TM domains (*4*−*7*); a heptad motif of leucines (*8*); a polar motif via the formation of hydrogen bonds (*9*−*13*), as well as tryptophan side chain (*14*).

The CD3/T-cell receptor (TCR) complex of the majority of the mature T-cells is a TCRα$\beta$ heterodimer associated with the $\gamma$, $\delta$, $\epsilon$, and $\zeta$ chains of CD3 (*15*). This complex is stabilized by interactions between the transmembrane domain of the TCR chains and CD3 subunits. The interaction of the TCR with a peptide presented by the major histocompatibility complex molecule (MHC) induces a conformational change in the TCR that triggers CD3 phosphorylation. Importantly, A 9 all-L-amino acids (aa) peptide derived from the trans membrane domain (TMD) of the TCRα chain, termed core peptide (CP[1]) (Figure 1), inhibits T-cell antigen specific activation *in vitro* and *in vivo* (*16*). CP has been shown to colocalize with the TCR molecules, inhibiting the proper assembly of the TCR-CD3 complex (*16*−*20*).

The interaction between CP and the CD3 complex is based on the interaction between the secondary structures and the side chains of the different components of these protein−protein complexes. However, the contribution of each one of these two factors has not been studied in detail (*21*, *22*). We have recently demonstrated that an α-helical mirror image peptide (all-D-CP) can associate with the native TMD of TCR to the same extent as the wild-type CP (*20*), probably via a structural rearrangement (a change in the interhelical angle) that occurs within the membrane to accommodate for the change in helix chirality. Such a structural adaptation raises questions with regard to the role of the secondary structure in the assembly process. A recent publication (*23*) reported that a hydrophobic region and a polar face were

† D.G.'s research is being supported by the Hughes and Sheila Potiker Postdoctoral Fellowship in Autoimmune Disease Research. This study was supported by the Israel Science Foundation.

* To whom correspondence should be addressed, at the Department of Biological Chemistry, The Weizmann Institute of Science, Rehovot, 76100 Israel. Tel: 972-8-9342711. Fax: 972-8-9344112. E-mail: Yechiel.Shai@weizmann.ac.il.

‡ Department of Immunology.

§ These two authors contributed equally to the work.

|| Department of Biological Chemistry.

[1] Abbreviations: AA, adjuvant arthritis; CD, circular dichroism; CP, TCRα transmembrane domain derived peptide; DMSO, dimethyl sulfoxide; DTH, delayed type hypersensitivity; IFA, incomplete Freund's adjuvant; LPC, lysophosphatidyl-choline; Mt, *Mycobacterium tuberculosis*; PPD, tuberculin-purified protein derivative; PC, phosphatidyl-choline.

10.1021/bi061849g CCC: $37.00 
Published on Web 02/09/2007

A

| Designation | Sequence |
|---|---|
| All-L CP (wild type) | GLRILLLKV |
| 2D CP[a] (diastereomer) | GLRILLLKV |
| 2G CP[b] (control) | GLGILLLGV |

[a]D-amino acids are underlined.
[b]The Gly mutations are in bold

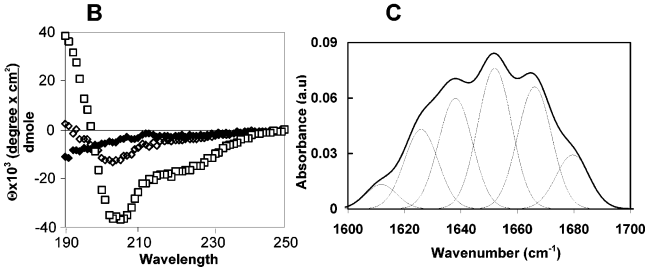


FIGURE 1: (A) Designation of peptides and their amino acid sequences. (B) CD spectra of all-L-CP in $H_2O$ (black diamonds), 2D-CP in 1% LPC micelles (empty diamonds), and all-L-CP in 1% LPC micelles (empty squares). 2D-CP in water did not yield a significant signal and therefore not shown. (C) FTIR spectra deconvolution of the fully deuterated amide I band (1600 to 1700 $cm^{-1}$) of 2D-CP in PC multibilayers. The thick line represents the experimental FTIR spectra after Savitzky−Golay smoothing; the thin lines represent the fitted components. A 200:1 lipid/diastereomer molar ratio was used.

required for the peptide to be active and that the amino acids were important in addition to charge. Charge alone was not fully responsible for these interactions, since shifting, switching, or replacing the positive charges within CP did not abolish activity completely. However, such changes by nature are likely to modify the topography of the structure. Thus, differences in activity may be also the result of the secondary structure and not the specific modification. Additional investigations are needed to better understand the role of the secondary structure in the function of CP.

To study the relative contributions of a secondary structure and side chains for the interaction between CP and the TCR/CD3, we introduced two D-amino acids in the positions of the two positive residues (2D-CP). Thus, we could severely perturb the secondary structure, while maintaining the original amino acid sequence. Note that these two side chains are important for the function and association of CP with the TCR (*15*−*18*). Recent studies have shown that these side chains are essential but not crucial, since some function persists despite displacement upward or downward in the sequence (*23*). Our data reveal that association of CP with the TCR complex is independent of secondary structure and is controlled mostly by side chain interactions. This observation has important clinical implications with regard to modulation of TCR and other receptor complexes, since D,L-amino acid containing peptides have better solubility and higher resistance to protease degradation.

## MATERIALS AND METHODS

*Peptide Synthesis and Fluorescent Labeling.* Peptides were synthesized by solid phase on PAM-amino acid resin (0.15 mequiv), as previously described (*24*, *25*). The synthetic peptides were purified (>98% homogeneity) by RP-HPLC on a $C_4$ column using a linear gradient of 20−60% acetonitrile in 0.05% TFA for 60 min. The peptides were subjected to amino acid analysis and mass spectrometry to confirm their composition. Unless stated otherwise, stock solutions of concentrated peptides in DMSO were used to avoid aggregation of the peptides before use. Resin-bound peptides were treated with 5-carboxytetramethylrhodamine, succinimidyl ester (Rhodamine-SE). The reaction with Rhodamine was in DMF containing 2% diisopropylethylamine. The fluorescent probe was used in an excess of 2 equiv, leading to the formation of resin bound N-terminal Rhodamine-labeled peptides (*26*, *27*). After 1 h, the resins were washed thoroughly with DMF and then with methylene chloride. All purified peptides were shown to be homogeneous (>98%) by analytical RP-HPLC (*26*).

*Fourier-Transform Infrared Spectroscopy (FTIR).* Spectra were obtained with a Bruker equinox 55 FTIR spectrometer equipped with a deuterated triglyceride sulfate (DTGS) detector and coupled with an ATR device, as previously described (*28*). Lipid−peptide mixtures, PC (0.5 mg) alone or with peptide (~20 $\mu$g), were prepared by dissolving them together in a 1:2 $MeOH/CH_2Cl_2$ mixture and drying under a stream of dry nitrogen. The mixtures were deposited on a ZnSe horizontal ATR prism (80 × 7 mm). Spectra were recorded, and the respective pure phospholipid spectrum was subtracted to yield the difference spectrum. Hydration of the sample was achieved by the introduction of excess deuterium oxide ($^2H_2O$) and incubation for 2 h prior to measurement of the spectra. H/D exchange was considered complete after a total shift of the amide II band. The spectra were processed using PEAKFIT (Jandel Scientific, San Rafael, CA) software as previously described in detail (*28*−*31*). Second-derivative spectra accompanied by 13-data-point Savitsky−Golay smoothing were calculated to identify the positions of the component bands in the spectra. These wavenumbers were used as initial parameters for curve fitting with Gaussian component peaks.

*Circular Dichroism Spectroscopy (CD).* The CD spectra of the peptides were measured in an Aviv 202 spectropolarimeter (Aviv, Lakewood, NJ). The spectra were scanned with a thermostated quartz optical cell with a path length of 1 mm. Each spectrum was recorded in 1 nm intervals with an averaging time of 20 s, at a wavelength range of 260 to 190 nm. The peptides were tested at a 50 $\mu$M concentration in either $H_2O$ or 1% LPC micelles.

*Molecular Dynamics Simulation.* The simulation system consists of 107 DMPC molecules, 3655 water molecules, and the investigated peptides (Figure 1). In order to keep the simulation box neutral, two water molecules were replaced with two counter Cl anions. The starting conformation of the DMPC membrane was downloaded from the group site of D. P. Tieleman at the University of Calgary (http://moose.bio.ucalgary.ca/index.php?page=Downloads). Simulation and data analysis were carried out using Gromacs 3.2.1 suite (*32*, *33*). The system was kept under constant pressure and temperature (NPT) weak coupling (*34*). Constant pressure of 1 bar was coupled independently, with coupling constant of $\tau_P = 1.0$ ps, to the three directions of the simulation box in order to allow the optimal molecular density. A temperature bath was coupled separately to the ions, water, lipid, and protein molecules at 310k and a coupling constant of $\tau_T = 0.1$ ps. A cutoff distance for the electrostatic and Lennard-Jones interactions was set to 15 Å and 12 Å, respectively. Atom neighbors list was updated

every 20 femtosecond (fs). The long-range electrostatic interactions were calculated using the Particle Mesh Ewald (PME) summation (*35*). Bond lengths were constrained using the LINCS algorithm (*36*). A modified version of the united-atoms GROMOS-96 force field was used (*37*) that was refined for better lipid parameters. All polar hydrogen atoms were treated explicitly, while aliphatic hydrogen atoms were implicitly described in the force field. The flexible simple point charge (SPC) water potential description (*38*) was used. The total simulation time was 10 ns, apart from the first 100 ps of restrained run. During the simulation a 2 fs time step was used. The CPU time was approximately 36 h per nanosecond on an Intel 2.7 GHz Xeon processor.

*Animals.* Two month old female Lewis rats were used. The rats were raised and maintained under pathogen-free conditions in the Animal Breeding Center of the Weizmann Institute of Science. Eight week old female BALB/c mice were maintained under similar pathogen-free conditions. The experiments were performed under the supervision and guidelines of the Institutional Animal Care and Use Committee of The Weizmann Institute of Science.

*Fluorescence Microscopy.* Activated A2b T-cells (*39*) ($10^5$ cells/sample) were incubated in 100 $\mu$L of PBS containing paraformaldehyde 4% for 15 min on ice. The samples were then washed with cold PBS and centrifuged for 7 min at 1100 rpm. PBS containing BSA 1% was then added at room temperature to prevent nonspecific binding. After 30 min FITC-labeled antibody against TCR was added at a dilution of 1:100 and incubated for 2.5 h. For colocalization of TCR with the peptide, Rhodamine 2D-CP was added at a final concentration of 1 $\mu$M (stock in DMSO) and incubated for 5 min. Samples were then washed once with PBS and loaded on a microscope slide. We used Rhodamine-labeled CP and 2G-CP as positive and negative controls, respectively.

The cells were then observed under a fluorescent confocal microscope. FITC excitation was set at 488 nm, with the laser set at 20% power to minimize bleaching of the fluorophore. Fluorescence data was collected from 505 to 525 nm. Rhodamine excitation was set at 543 nm, with the laser set at 5% power. Fluorescence data was collected from 560 nm and up.

Fluorescence energy transfer between the FITC (donor) and Rhodamine (acceptor) was detected as an increase in FITC fluorescence in an area where the Rhodamine probe was bleached. Bleaching was achieved by point excitation at 543 nm for 6 s with the laser set to 100%. To verify that the increase in FITC fluorescence is not due to autofluorescence, we bleached using the 488 nm laser first and only then at 543 nm. No signal was observed in either 505−525 nm or >560, eliminating the possibility of autofluorescence.

*Co-Immunoprecipitation of Fluorescently-Labeled Peptides with TCR Molecules.* Activated A2b T-cells ($2 \times 10^6$) were cultured for 1 h at 37 °C in the presence of CP or 2D-CP (25 $\mu$g/mL), or 2G-CP, and lysed for 15 min on ice in 0.1 mL of lysis buffer (*40*). Insoluble material was removed by centrifugation at 10000*g* for 10 min at 4 °C. The lysate was then incubated overnight with Protein A-plus Agarose beads (Santa Cruz Biotechnology Inc., Santa Cruz, CA) bound to antibodies to the rat TCR or MHC class I. The antibodies reactive against the rat TCR (clone R73) were purified from the respective hybridomas at our lab. Antibodies to rat MHC class I were purchased from Serotec (Oxford, U.K.). After an overnight incubation at 4 °C, the beads were washed with lysis buffer and boiled for 10 min and the protein supernatant was run in a 4−20% SDS−PAGE. The presence of co-immunoprecipitated peptide was detected by the Typhoon 9400 variable mode imager.

*T-Cell Proliferation.* T-cell proliferation assays were performed using LNC from rats immunized with *Mycobacterium tuberculosis* (Mt). Popliteal and inguinal LNC were removed 26 days after the injection of Mt in incomplete Freund's adjuvant (IFA), when strong T-cell responses to tuberculin-purified protein derivative (PPD) and the Mt176-90 peptide of the 65 kDa heat shock protein (HSP65) (*41*) are detectable. LNC were cultured at a concentration of $2 \times 10^5$ cells per well; $5 \times 10^4$ A2b T-cells were stimulated in the presence of irradiated $5 \times 10^5$ thymic antigen presenting cells per well, prepared as previously described (*42*). The cells were plated in quadruplicates in 200 $\mu$L round-bottom microtiter wells, with or without antigen, in the presence of various concentrations of the peptides under study and PPD or Mt176-90. Cultures were incubated for 72 h at 37 °C in a humidified atmosphere of 7.5% $CO_2$. T-cell responses were detected by the incorporation of [methyl-$^3$H]-thymidine (Amersham, Buckinghamshire, U.K.; 1 $\mu$Ci/well), added during the last 18 h of incubation. The results of T-cell proliferation experiments are shown as the % of inhibition relative to the T-cell proliferation triggered with antigen stimulation in the absence of peptides.

*Induction and Assessment of Adjuvant Arthritis* (*AA*). To test the effect of CP on T-cell activation *in vivo*, we used the experimental T-cell mediated autoimmune disease AA. AA was induced by injecting 50 $\mu$L of Mt suspended in IFA (10 mg/mL) at the base of the tail. At the time of AA induction, each rat also received 100 $\mu$g of all-L-CP, 2D-CP, or 2G-CP control peptide (or PBS) dissolved in 50 $\mu$L of IFA and mixed with the Mt/IFA used to induce AA. The day of AA induction was designated as day 0. Disease severity was assessed by direct observation of all 4 limbs in each animal. A relative score between 0 and 4 was assigned to each limb, based on the degree of joint inflammation, redness, and deformity; thus the maximum possible score for an individual animal was 16 (*41*). The mean AA score (± SEM) is shown for each experimental group (6 rats per group). Arthritis was also quantified by measuring hind limb diameter with a caliper. Measurements were taken on the day of the induction of AA and 26 days later (at the peak of AA); the results are presented as the mean diameter ± SEM of the difference between day 26 and day 0 for all the animals in each group. The person who scored the disease was blinded to the identity of the groups.

*Delayed Type Hypersensitivity to PPD.* Twenty microliters of PPD (0.5 mg/mL in PBS) were injected intradermally into the pinna of the right ear on day 16 after AA induction; 20 $\mu$L of sterile PBS was injected into the left ear as control. The thickness of the ear was measured 48 h later using a vernier caliper and expressed as the difference between the right and the left ear (*43*).

*Delayed Type Hypersensitivity to Oxazalone.* Groups of 5 female inbred BALB/c mice (The Jackson Laboratory) were sensitized on the shaved abdominal skin with 100 $\mu$L of 2% oxazalone dissolved in acetone/olive oil [4:1 (vol/vol)] applied topically. DTH sensitivity was elicited 5 days later by challenging the mice with 20 $\mu$L of 0.5% oxazalone

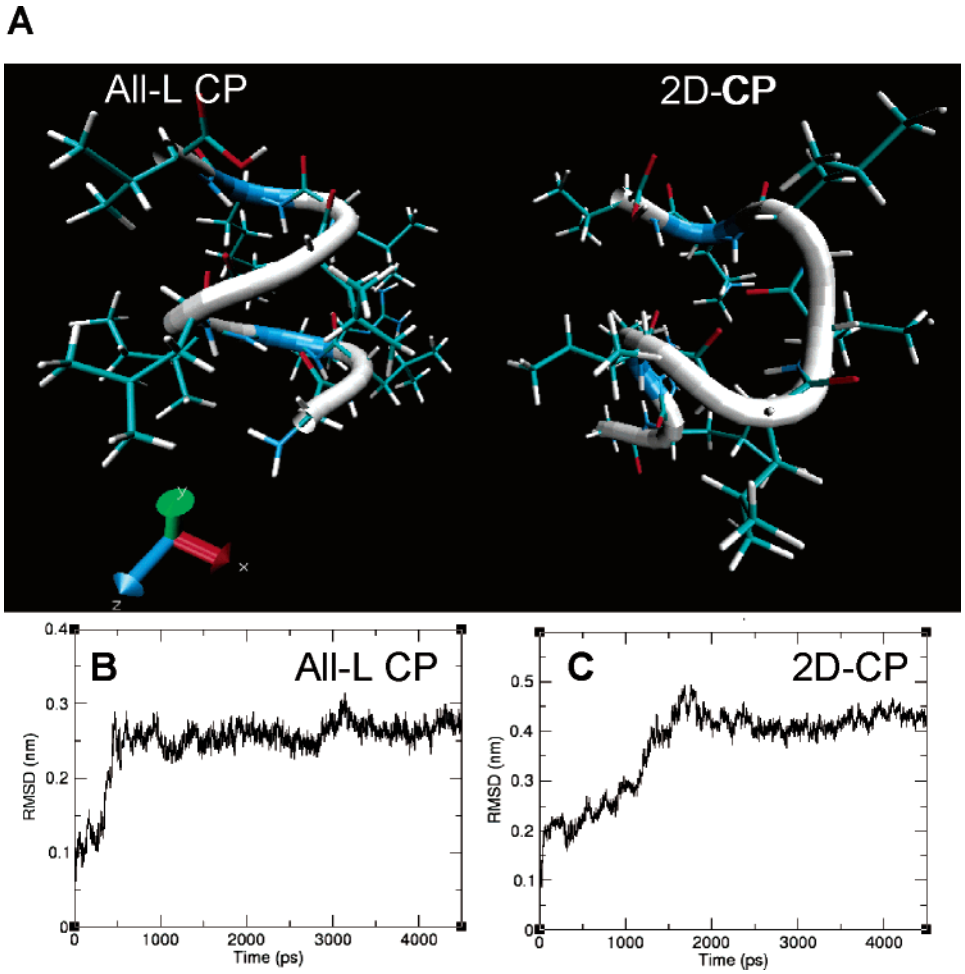


FIGURE 2: (A) Structures generated for all-L-CP and 2D-CP by molecular dynamics simulation showing that D aa disturb the α-helical structure of CP in a bilayer model. (B) All atom rmsd profile across the first 5 ns of the simulation of all-L-CP in the lipid bilayer. (C) The rmsd profile of 2D-CP.

in acetone/olive oil, 10 $\mu$L administered topically to each side of the ear. A constant area of the ear was measured immediately before challenge and 24 h after challenge with a Mitutoyo engineer's micrometer. The individual measuring ear swelling was unaware of the identity of the groups of mice. The DTH reaction is presented as the increment of ear swelling after challenge expressed as the mean ± SEM in units of $10^{-2}$ mm. One hour after the challenge the mice's ears were treated with either all-L-CP or 2D-CP, both dissolved in 40 $\mu$L of DMSO. The activity of the peptide treatments was compared to treatment with DMSO alone for "untreated mice" and dexamethasone (100 $\mu$g/mL in saline) as a positive control.

*Statistical Significance.* The InStat 2.01 program (Graph Pad Software, San Diego, CA) was used for statistical analysis. Student's *t* test and the Mann−Whitney *U* test (two tailed) were used to determine significance of the differences between groups.

## RESULTS

We replaced the two positive residues of CP (Arg and Lys) with their D-enantiomers (2D-CP) in order to destabilize the secondary structure while keeping the aa sequence. In addition, to test for sequence specificity we synthesized a mutant in which the two positive residues were mutated to glycines (*16*, *20*). Figure 1A lists the designations and aa sequences of the peptides used in this study.

*The 2D-CP Lacks a Stable α-Helical Structure as Revealed by Circular Dichroism (CD) Spectroscopy, Fourier-Transform Infrared Spectroscopy (FTIR), and Molecular Dynamics Simulation.* CD experiments were carried out under two experimental conditions: in $H_2O$ and in 1% lysophosphatidyl-choline (LPC) micelles which mimic membrane environment. Figure 1B shows the CD spectra of CP in water (filled diamonds), 2D-CP in micelles (empty diamonds), and all-L-CP in micelles. The spectra of 2D-CP in water yielded only the background signal and therefore are not shown. The data reveal that the all-L-CP has α-helical secondary structure in micelles, similar to previous reports (*20*, *44*), whereas no significant secondary structure was observed for the 2D-CP peptide, as expected.

The structure of 2D-CP was determined also by FTIR (Figure 1C). The data reveal a significantly altered structure for 2D-CP. Deconvolution of the signal resulted in 6 different peaks for this 9 aa peptide. Therefore, we can conclude that 2D-CP does not have a significant helical structure. These data confirm the CD spectroscopy results.

The stability of the secondary structures of all-L-CP and 2D-CP was further compared by running a molecular dynamics simulation in a lipid bilayer model for 10 ns

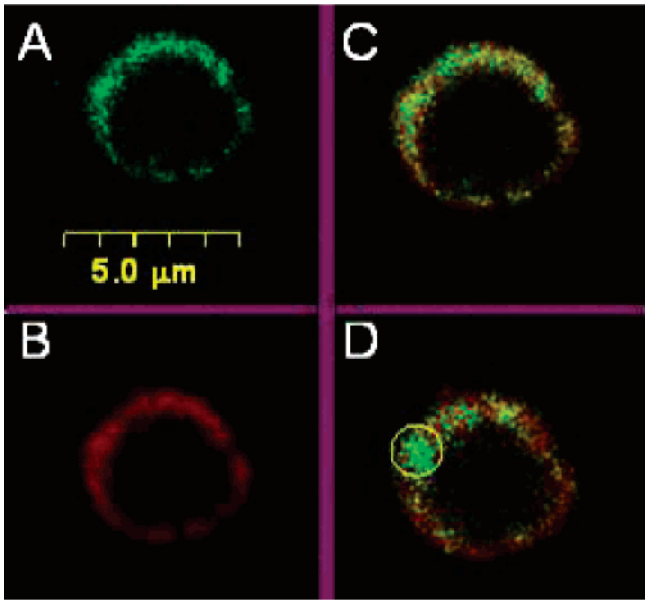


FIGURE 3: The 2D-CP peptide colocalizes with the TCR receptor. (A) The TCR is visualized using a TCR-FITC antibody. Excitation was at 488 nm, and the emission was collected between 505 and 525 nm. (B) The 2D-CP was visualized using a Rhodamine probe attached to the N-terminus. Excitation was at 543 nm, and emission was collected from 560 nm and up. (C) Merging of the two channels before bleach demonstrates that the 2D-CP colocalizes with the TCR. (D) The yellow circle surrounds the area which underwent bleaching. Bleaching was achieved with the laser (543 nm) set at 100% power for 6 s. Thus, the FITC donor molecule was not affected. The increase in green demonstrates that there was fluorescence energy transfer between the Rhodamine-labeled 2D-CP peptide and the TCR-FITC.

(Figure 2A). The comparison of the secondary structures resulting from the molecular dynamics simulation indicates that all-L-CP maintains its α-helical structure, which is lost in the 2D-CP mutant (Figure 2A). The root-mean-square deviation (rmsd) increases as a molecular structure departs from its initial structure, and it reaches a plateau once a new stable conformation has been acquired. When the rmsd for the two peptides was compared, the data revealed that both the wild-type all-L-CP and 2D-CP equilibrated after about 4 ns in the lipid bilayer (Figure 2B, 2C). Moreover, the rmsd calculated over the equilibrated phase is 0.25 nm (Figure 2B) and 0.4 nm (Figure 2C) for all-L-CP and 2D-CP, respectively. The rmsd of 2D-CP is 62.5% higher than that of all-L-CP, again indicating that 2D-CP displays a secondary structure that is less stable than that of all-L-CP. There was no significant difference in the effect of the two peptides on the membrane density after insertion into the bilayer. In summary, the results of the CD spectroscopy and computational analysis indicate that the two D aa disrupt the right-handed α-helical structure adopted by the all-L-CP peptide as expected.

*The α-Helical Structure of CP Is Not Required for T-Cell Binding and Localization.* The CP peptide has been described to insert itself into the CD3/TCR complex and interfere with the activation of T-cells triggered by their cognate antigen (*16*−*18*). Here we investigated the localization of Rhodamine-labeled 2D-CP and TCR-specific FITC-labeled antibodies (αTCR-FITC) on the T-cell membrane. Figure 3C depicts the colocalization of αTCR-FITC (Figure 3A) and Rhodamine 2D-CP (Figure 3B), suggesting that the 2D-CP analogue

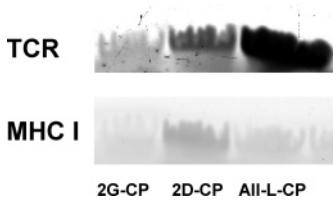


FIGURE 4: Both all-L-CP and 2D-CP co-immunoprecipitate together with the TCR. We incubated either all-L-CP, 2D-CP, or 2G-CP together with activated A2B cells and immunoprecipitated either the (a) TCR or (b) MHC I molecules. all-L-CP and 2D-CP co-immunoprecipitated together with the TCR significantly more than the 2G-CP mutant. The peptides did not co-immunoprecipitate together with the MHC I molecule to any significant extent. We used the mouse IgG1 antibody anti-rat αβ TCR (TCR αβ), clone R73 provided by eBioscience (San Diego, CA) (catalog No. 16-5960). The MW range is in the peptide size 1−10 Kd. The band is observed at around 1 Kd, which is the correct range for the size of the all-L-CP peptides.

inserts into the T-cell membrane and colocalizes with the TCR, as was seen with wild-type CP (*17*, *20*).

To confirm these colocalization results, fluorescence energy transfer experiments were performed between Rhodamine 2D-CP and αTCR-FITC. For that purpose, a 543 nm laser was used to irradiate a point on the T-cell membrane that exhibited high intensity of both Rhodamine 2D-CP and αTCR-FITC, bleaching the signal produced by the Rhodamine 2D-CP, but leaving intact the emission produced by the αTCR-FITC. This procedure led to a significant increase in the fluorescence of the αTCR-FITC shown in Figure 3D. To rule out autofluorescence as a source of increased signal in the 505−525 nm range, we used two controls. First, we bleached the same position with the 488 nm laser. This resulted in complete bleaching of the signal, suggesting that the fluorescence increase seen above was generated by the FITC probe and did not result from autofluorescence in the sample. Second, we chose a point on the surface of cells stained with Rhodamine 2D-CP and αTCR-FITC that showed no fluorescent signal and bleached it with the 543 nm laser. No increase in the FITC fluorescence was observed, ruling out autofluorescence as a source of fluorescence in the range of FITC. Overall, these results confirm that wild-type CP and its 2D-CP stereoisomer show the same localization in the T-cell membrane regardless of their differences in secondary structure.

*The 2D-CP Co-Immunoprecipitates Together with the TCR.* The interactions within the pairs TCR/CP, TCR/2D-CP, and TCR/2G-CP were investigated by performing a series of coprecipitation experiments using different concentrations of Rho-labeled CP, 2D-CP, and 2G-CP peptides. Figure 4 shows that both CP and 2D-CP can be coprecipitated with the TCR, although the TCR/CP interaction seems to be stronger. The difference in the intensities of CP and 2D-CP could result from their different oligomeric states, as suggested by FRET (data not shown). This would lead to a different equilibrium with the TCR complex. Nevertheless, both CP and 2D-CP interact with the TCR significantly more than the 2G-CP mutant. On the other hand, none of the peptides significantly coprecipitated together with the MHC I molecule that was used as a control surface protein. These results further support specific interaction of 2D-CP with the TCR molecule. The A2b T-cell line used in our studies (and rat T-cells in general) expresses high levels of MHC

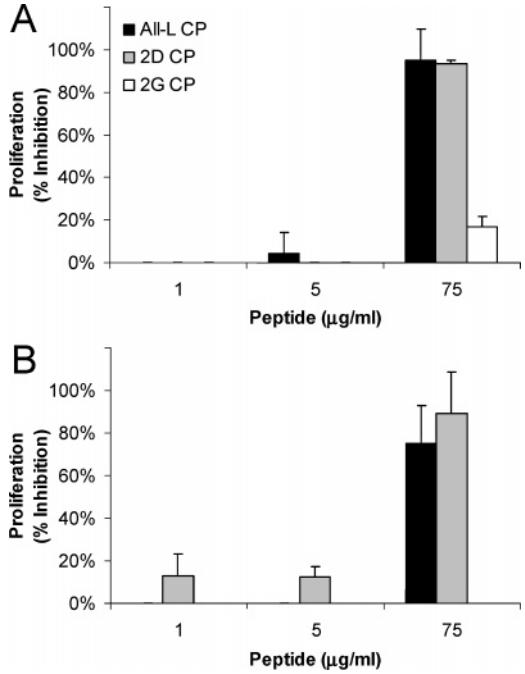


FIGURE 5: 2D-CP peptide interferes with T-cell activation. LNC from Mt primed rats were activated *in vitro* with PPD (A) or with Mt176-90 (B), in the presence of wild-type all-L-CP (black), 2D-CP (gray), or 2G-CP (white).

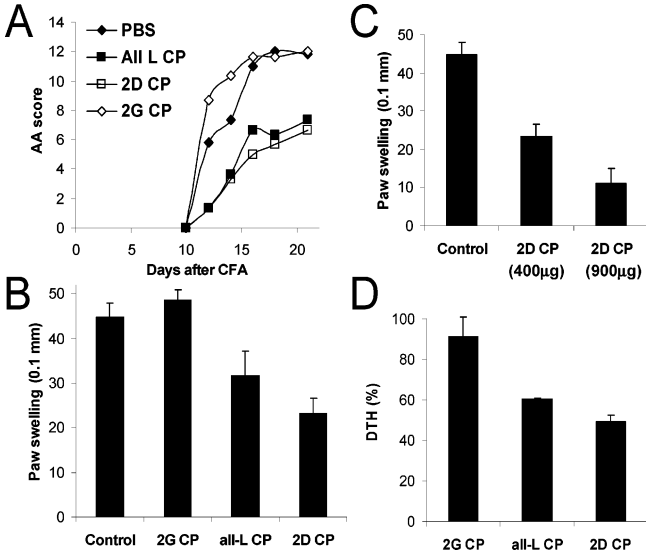


FIGURE 6: Inhibition of AA by all-L-CP and 2D-CP. Adjuvant arthritis was induced with Mt in oil, mixed with all-L-CP (all-L-CP), 2D-CP, 2G-CP, or PBS. Arthritis was scored every 2−3 days, starting at day 10. (A) Time course of the AA score, presented as the mean ± SEM. $p < 0.05$ when the results of 2D-CP or all-L-CP treated animals are compared with those of the control groups treated with PBS or 2G-CP. (B) Paw swelling measured at day 26 after AA induction. The results are presented as the mean ± SEM of the difference between the values for hind limb diameter taken at days 0 and 26. $p < 0.05$ between the control groups treated with PBS or 2G-CP and all-L or 2D-CP treated rats. (C) Dose dependency of the effect of the 2D-CP on AA, as measured by paw swelling at day 26. (D) DTH was measured as described in Materials and Methods to quantify the effect of the peptides on the immune response to Mt. The results are expressed as percent of the uninhibited DTH response to Mt. The reduction observed on rats treated with all-L-CP or 2D-CP is significant ($p < 0.05$) when compared to the effect of 2G-CP.

class I molecules (*45*, *46*); indeed a comparison of the MHC class I and TCR expression has shown that TCR and MHC I molecules are expressed at similar levels by rat T-cells using the same antibodies as in the co-immunoprecipitation experiment (*47*). Moreover, the procedure for the immunoprecipitation of MHC class I molecules with the Ox18 antibody has been used in our laboratory to determine the binding motifs of MHC class I rat molecules. Thus, the differences shown in Figure 4 between co-immunoprecipitation with antibodies to TCR or MHC cannot be due to differences in the amounts of cellular receptors.

*2D-CP Interferes with T-Cell Activation in Vitro.* The colocalization studies (Figure 3) suggested that the secondary structure of CP was not essential for its ability to insert into the T-cell membrane and interact with the CD3/TCR complex. To test whether the secondary structure of CP contributed to its interference with the activation of T-cells by antigen, we isolated lymph node cells (LNC) from Mt-immunized rats and activated the T-cells *in vitro* with PPD or with the Mt176-90 peptide. Both PPD and Mt176-90 have been reported to induce a strong T-cell proliferative response in the LNC of Mt-immunized rats (*41*, *48*). The data reveal that both wild-type all-L-CP and 2D-CP inhibited T-cell proliferation to PPD and to Mt176-90 in a dose-dependent manner (Figure 5). Note, however, that at lower concentrations, the inhibition of 2D-CP was greater ($p < 0.02$) than that produced by all-L-CP (Figure 5B). Conversely, the 2G-CP mutant did not have any inhibitory effect on T-cell proliferation, suggesting that inhibition was sequence specific and that critical molecular interactions were perturbed by the substitution of two positive aa for Gly residues (see Figure 1). Thus, the precise secondary structure of CP does not seem to be required for its inhibitory effects on T-cell activation, which remained dependent on various side chain interactions. Recently, an NMR structure of CD3 zeta in a detergent revealed that the CD3 acidic residues are not charged and actually form a strong polar bond with each other's backbone (*49*). We do not know exactly how the R and K behave in the membrane. Therefore, we refer to a side chain without making a distinction between polarity and geometry of the aa residue. None of the peptides (all-L-CP, 2D-CP, or 2G- CP) had a cytotoxic effect when incubated with the target cells, ruling out that the effects on antigen-triggered proliferation were due to cell death (data not shown).

*2D-CP Inhibits T-Cell Immunity in Vivo.* To analyze the effect of structure alteration on the inhibitory effects of CP on T-cell activation *in vivo*, we used the experimental autoimmune disease AA. Immunization of Lewis rats with Mt triggers AA, an autoimmune disease driven by Mt-specific T-cells that cross-react with self-antigen (*50*, *51*). PPD and Mt176-90 are targeted by the arthritogenic T-cell response (*52*); indeed immunomodulatory therapies that inhibit the progression of arthritis have been associated with a decreased T-cell response to PPD and Mt176-90 and with a diminished delayed type hypersensitivity (DTH) response to PPD (*42*).

The administration of all-L-CP or 2D-CP with Mt at the time of AA induction led to a significantly milder arthritis, in terms of both clinical score (Figure 6A) and paw swelling (Figure 6B); the 2G-CP peptide did not have an effect on AA. The mean maximum score was 12 ± 0.3 in the 2G-CP-treated rats, compared with 6.6 ± 0.7 in the 2D-CP-

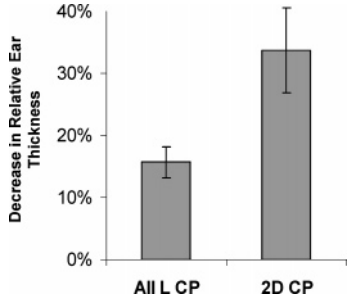


FIGURE 7: 2D-CP inhibits DTH response to oxazalone in mice. DTH response measured 1 h after challenge with oxazalone of mice treated with DMSO alone used as a control, all-L-CP, 2D-CP, or dexamethasone. The results are expressed as the decrease in ear thickness obtained after treatment with the peptides, relative to the decrease observed in dexamethasone-treated mice (which was considered 100%), ± SEM.

treated rats and 7.7 ± 0.7 in the all-L-CP group ($p < 0.05$ for the all-L-CP and the 2D-CP groups when compared to the 2G-CP group). The effect of 2D-CP on AA was dose dependent, since an increase of the dose of 2D-CP to 900 μg per rat led to a further 25% decrease in the AA score (data not shown) and a 50% improvement in paw swelling (Figure 6C). The study of the DTH response to PPD 16 days after AA induction revealed that the administration of wild-type all-L-CP or 2D-CP led to a 39% and 51% reduction in the DTH response to PPD, respectively. In comparison, treatment with 2G-CP led only to an 8.5% inhibition of the DTH response. Taken together, these results indicate that both the 2D-CP and wild-type all-L-CP can interfere *in vivo* with T-cell activation in a sequence specific manner that was, nevertheless, independent of the secondary structure of the peptide.

*2D-CP Decreases the DTH Response in a Therapeutic Setting.* To test whether TCR trans-membrane peptides could inhibit the elicitation of existing DTH reactivity, groups of naive BALB/c mice were sensitized to 2% oxazalone. Five days later, the mice were challenged with 0.5% oxazalone administered to the ear. An hour after the challenge, the mice were treated with dimethyl sulfoxide (DMSO), all-L-CP 150 μg (6 mg/kg) in DMSO, 2D-CP 150 μg (6 mg/kg) in DMSO, or dexamethasone. On the following day, ear thickness was measured and the swelling of DMSO treated mice (0.33 ± 0.01 mm) was compared to that of mice treated with all-L-CP (0.30 ± 0.01 mm), 2D-CP (0.27 ± 0.01 mm), and dexamethasone (0.15 ± 0.02 mm). A significant reduction in ear swelling was observed in the mice that had been treated with 2D-CP ($p < 0.01$ when compared to the DMSO group); indeed, 2D-CP caused twice the reduction produced by treatment with all-L-CP ($p < 0.05$ when compared to the DMSO group) (Figure 7). Thus, 2D-CP can inhibit a T-cell mediated immune reaction in subjects already sensitized to the antigen.

## DISCUSSION

Wild-type all-L-CP interferes with antigen-specific T-cell activation by interacting with the TCR complex (*16*−*18*). This interaction was thought to depend both on the secondary structure of CP and on the side chains of its two positive residues (Figure 1), since their substitution by glycines or a negatively charged aa abolishes the peptide's activity (*16*, *19*). In this report we investigated the molecular interactions that mediate the immunosuppressive activity of CP, using structural analogues in which its two positive residues were replaced by D aa. These analogues have the same aa sequence, but display severe perturbations of their secondary structure. We found, indeed, that the introduction of two D aa destabilized the helical secondary structure within the membrane milieu, as shown by the CD spectra (Figure 1B), by the FTIR spectra (Figure 1C), and by the molecular dynamics simulation (Figure 2). The 2D-CP also has an increased water solubility and shorter RP-HPLC retention time compared with CP (data not shown). Nevertheless, 2D-CP colocalized with the TCR complex in the T-cell membrane (Figure 3), co-immunoprecipitated together with the TCR, and interfered with T-cell activation (Figures 4, 5, 6, and 7). This suggests that the immunosuppressive activity of CP is determined by side chain interactions and that the α-helical structure is not crucial for this interaction.

Despite the observation that the two D aa introduced in CP perturb its secondary structure (Figure 1), upon binding to the membrane the 2D-CP peptide displays wild-type functionality. One possibility is that 2D-CP adopts an alternative stable structure within the membrane, different from that of all-L-CP. Previous reports have shown that the hydrophobic environment of the membrane stabilizes the α-helical structure of other TMD and antimicrobial amphipathic diastereomeric peptides, probably as a result of the massive energy released with the adoption of a secondary structure within the membrane (*53*−*55*). Our data suggest that 2D-CP does not preserve the same structure as that of CP within the membrane (Figures 1B, 2). Nevertheless, the activity of the mutant CP 2D peptide still relies on molecular interactions established by its two positive aa L-arginine and L-lysine, because their replacement by glycines abolishes the immunosuppressive activity (Figures 4 and 5).

Remarkably, the diastereomeric peptide 2D-CP showed a stronger immunosuppressive activity than did wild-type all-L-CP. *In vitro*, 2D-CP was more active at lower concentrations than all-L-CP (Figure 5). *In vivo*, the administration of 2D-CP led to a greater reduction in the clinical signs of AA when compared to the all-L-CP (Figure 6). Moreover, 2D-CP was twice more effective than all-L-CP when used to inhibit a DTH response in a therapeutic setting. Note that 2D-CP, similarly to what we have previously shown for CP (*44*), is not cytotoxic *in vitro* (data not shown). Two features of 2D-CP common to other diastereomeric peptides might contribute to its relatively enhanced immunosuppressive activity. These are higher solubility in water (*56*) and increased resistance to degradation (*57*). Both characteristics would contribute *in vivo* to better transport of the peptide through the tissue to their target T-cells. CP is hydrophobic and has been already shown to bind both zwitterionic and negatively charged model phospholipid membranes (*19*). The incorporation of D-amino acids makes it more soluble, but should preserve strong binding to the membrane as has been shown with other membrane active peptides. CP then inserts and interacts with a TM domain within the TCR complex.

The association of glycophorin A TMD with its diastereomeric mutant *in vitro* to form a heterodimer is another example of a membrane complex whose formation is dictated by side chain interactions and not solely by secondary structure (*27*). Yet, there are significant differences in the nature of the two systems. The glycophorin A receptor is a

homodimer while the TCR is a large hetero-oligomer. The glycophorin A diastereomer retained its helical structure while the 2D-CP did not. The latter could be explained by the different length of the peptides, glycophorin A (17 aa) versus CP (9 aa), by the large number of Gly, which makes the structure more flexible, and by the presence of two charged aa in CP. Such positive charges are very rare in TMD motifs. Nevertheless, the similarity of complex formation with the diastereomeric peptide in the membrane, regardless of the different nature of the complexes, is intriguing. It raises the question of whether TMD−TMD association is, as a general rule, governed by side chain interactions (of all types) while secondary structure and geometrical packing of the helices (knob-into-hole interactions) play a role in stabilizing the complex. Additional studies are required to address these questions.

In summary, to our knowledge the present study is the first report of a D,L-amino acid TM peptide inhibitor interacting both *in vitro* and *in vivo*, with a large transmembrane complex independent of its secondary structure. This observation has implications for our understanding of protein association within the membrane milieu. Moreover, this finding might make it possible to design more effective therapeutic diastereomeric peptides that, by a peptide displacement strategy, could interfere with the association and signal transduction of protein complexes, thereby deactivating pathologic processes.

## ACKNOWLEDGMENT

We thank Vladimir Kiss for his help with the confocal microscopy, Batya Zarmi for peptide purification, and Sergio G. Peisajovich for his helpful suggestions. Y.S. has the Harold S. and Harriet B. Brady Professorial Chair in Cancer Research. I.R.C. is the Mauerberger Professor of Immunology at the Weizmann Institute of Science, and the Director of the Center for the Study of Emerging Diseases, Jerusalem.

## REFERENCES

1. DeGrado, W. F., Gratkowski, H., and Lear, J. D. (2003) How do helix-helix interactions help determine the folds of membrane proteins? Perspectives from the study of homo-oligomeric helical bundles, *Protein Sci. 12*, 647−665.
2. Stevens, T. J., Mizuguchi, K., and Arkin, I. T. (2004) Distinct protein interfaces in transmembrane domains suggest an in vivo folding model, *Protein Sci. 13*, 3028−3037.
3. Li, E., and Hristova, K. (2006) Role of receptor tyrosine kinase transmembrane domains in cell signaling and human pathologies, *Biochemistry 45*, 6241−6251.
4. Lemmon, M. A., Flanagan, J. M., Hunt, J. F., Adair, B. D., Bormann, B. J., Dempsey, C. E., and Engelman, D. M. (1992) Glycophorin A dimerization is driven by specific interactions between transmembrane alpha-helices, *J. Biol. Chem. 267*, 7683−7689.
5. Lemmon, M. A., Treutlein, H. R., Adams, P. D., Brunger, A. T., and Engelman, D. M. (1994) A dimerization motif for transmembrane alpha-helices, *Nat. Struct. Biol. 1*, 157−163.
6. Russ, W. P., and Engelman, D. M. (2000) The GxxxG motif: a framework for transmembrane helix-helix association, *J. Mol. Biol. 296*, 911−919.
7. Saddar, S., and Stuart, R. A. (2005) The yeast F(1)F(0)-ATP synthase: analysis of the molecular organization of subunit g and the importance of a conserved GXXXG motif, *J. Biol. Chem. 280*, 24435−24442.
8. Gurezka, R., Laage, R., Brosig, B., and Langosch, D. (1999) A heptad motif of leucine residues found in membrane proteins can drive self-assembly of artificial transmembrane segments, *J. Biol. Chem. 274*, 9265−9270.
9. Choma, C., Gratkowski, H., Lear, J. D., and DeGrado, W. F. (2000) Asparagine-mediated self-association of a model transmembrane helix, *Nat. Struct. Biol. 7*, 161−166.
10. Zhou, F. X., Merianos, H. J., Brunger, A. T., and Engelman, D. M. (2001) Polar residues drive association of polyleucine transmembrane helices, *Proc. Natl. Acad. Sci. U.S.A. 98*, 2250−2255.
11. Dawson, J. P., Weinger, J. S., and Engelman, D. M. (2002) Motifs of serine and threonine can drive association of transmembrane helices, *J. Mol. Biol. 316*, 799−805.
12. Gratkowski, H., Lear, J. D., and DeGrado, W. F. (2001) Polar side chains drive the association of model transmembrane peptides, *Proc. Natl. Acad. Sci. U.S.A. 98*, 880−885.
13. Sal-Man, N., Gerber, D., and Shai, Y. (2005) The identification of a minimal dimerization motif QXXS that enables homo- and hetero-association of transmembrane helices in vivo, *J. Biol. Chem. 280*, 27449−27457.
14. Ridder, A., Skupjen, P., Unterreitmeier, S., and Langosch, D. (2005) Tryptophan supports interaction of transmembrane helices, *J. Mol. Biol. 354*, 894−902.
15. Call, M. E., Pyrdol, J., Wiedmann, M., and Wucherpfennig, K. W. (2002) The organizing principle in the formation of the T cell receptor-CD3 complex, *Cell 111*, 967−979.
16. Manolios, N., Collier, S., Taylor, J., Pollard, J., Harrison, L. C., and Bender, V. (1997) T-cell antigen receptor transmembrane peptides modulate T-cell function and T cell-mediated disease, *Nat. Med. 3*, 84−88.
17. Wang, X. M., Djordjevic, J. T., Bender, V., and Manolios, N. (2002) T cell antigen receptor (TCR) transmembrane peptides colocalize with TCR, not lipid rafts, in surface membranes, *Cell Immunol. 215*, 12−19.
18. Wang, X. M., Djordjevic, J. T., Kurosaka, N., Schibeci, S., Lee, L., Williamson, P., and Manolios, N. (2002) T-cell antigen receptor peptides inhibit signal transduction within the membrane bilayer, *Clin. Immunol. 105*, 199−207.
19. Bender, V., Ali, M., Amon, M., Diefenbach, E., and Manolios, N. (2004) T cell antigen receptor peptide-lipid membrane interactions using surface plasmon resonance, *J. Biol. Chem. 279*, 54002−54007.
20. Gerber, D., Quintana, F. J., Bloch, I., Cohen, I. R., and Shai, Y. (2005) D-enantiomer peptide of the TCR alpha transmembrane domain inhibits T-cell activation in vitro and in vivo, *FASEB J. 19*, 1190−1192.
21. Roy, R., Laage, R., and Langosch, D. (2004) Synaptobrevin transmembrane domain dimerization-revisited, *Biochemistry 43*, 4964−4970.
22. Stouffer, A. L., Nanda, V., Lear, J. D., and DeGrado, W. F. (2005) Sequence determinants of a transmembrane proton channel: an inverse relationship between stability and function, *J. Mol. Biol. 347*, 169−179.
23. Ali, M., Salam, N., Amon, M., Bender, V., Hibbs, D., and Manolios, N. (2006) T-Cell Antigen Receptor-alpha Chain Transmembrane Peptides: Correlation between Structure and Function, *Int. J. Pept. Res. Ther.*, in press.
24. Kliger, Y., Aharoni, A., Rapaport, D., Jones, P., Blumenthal, R., and Shai, Y. (1997) Fusion peptides derived from the HIV type 1 glycoprotein 41 associate within phospholipid membranes and inhibit cell-cell Fusion. Structure-function study, *J. Biol. Chem. 272*, 13496−13505.
25. Merrifield, R. B., Vizioli, L. D., and Boman, H. G. (1982) Synthesis of the antibacterial peptide cecropin A (1-33), *Biochemistry 21*, 5020−5031.
26. Gerber, D., and Shai, Y. (2000) Insertion and organization within membranes of the delta-endotoxin pore- forming domain, helix 4-loop-helix 5, and inhibition of its activity by a mutant helix 4 peptide, *J. Biol. Chem. 275*, 23602−23607.
27. Gerber, D., Pritsker, M., Gunther-Ausborn, S., Johnson, B., Blumenthal, R., and Shai, Y. (2004) Inhibition of HIV-1 Envelope Glycoprotein-mediated Cell Fusion by a DL-Amino Acid-containing Fusion Peptide: POSSIBLE RECOGNITION OF THE FUSION COMPLEX, *J. Biol. Chem. 279*, 48224−48230.
28. Oren, Z., and Shai, Y. (2000) Cyclization of a cytolytic amphipathic alpha-helical peptide and its diastereomer: effect on structure, interaction with model membranes, and biological function, *Biochemistry 39*, 6103−6114.
29. Jackson, M., and Mantsch, H. H. (1995) The use and misuse of FTIR spectroscopy in the determination of protein structure, *Crit. Rev. Biochem. Mol. Biol. 30*, 95−120.

30. Frey, S., and Tamm, L. K. (1991) Orientation of melittin in phospholipid bilayers. A polarized attenuated total reflection infrared study, *Biophys. J. 60*, 922−930.
31. Hong, J., Oren, Z., and Shai, Y. (1999) The Structure and Organization of Hemolytic and Nonhemolytic Diastereomers of Antimicrobial Peptides in Membranes, *Biochemistry 38*, 16963−16973.
32. Berendsen, H. J. C., Vanderspoel, D., and Vandrunen, R. (1995) Gromacs−a Message-Passing Parallel Molecular-Dynamics Implementation, *Comput. Phys. Commun. 91*, 43−56.
33. Lindahl, E., Hess, B., and van der Spoel, D. (2001) GROMACS 3.0: a package for molecular simulation and trajectory analysis, *J.Mol. Model. 7*, 306−317.
34. Berendsen, H. J. C., Postma, J. P. M., Vangunsteren, W. F., Dinola, A., and Haak, J. R. (1984) Molecular-Dynamics with Coupling to an External Bath, *J. Chem. Phys. 81*, 3684−3690.
35. Darden, T., York, D., and Pedersen, L. (1993) Particle Mesh Ewald−an N.Log(N) Method for Ewald Sums in Large Systems, *J. Chem. Phys. 98*, 10089−10092.
36. Hess, B., Bekker, H., Berendsen, H. J. C., and Fraaije, J. G. E. M. (1997) LINCS: A linear constraint solver for molecular simulations, *J. Comput. Chem. 18*, 1463−1472.
37. van Gunsteren, W. F., Billeter, S. R., Eising, A. A., Hünenberger, P. H., Krüger, P., Mark, A. E., Scott, W. R. P., and Tironi, I. G. (1996) pp 1−1024, Hochschulverlag AG an der ETH, Zurich, Switzerland.
38. Berendsen, H. J. C., Postma, J. P. M., van Gunsteren, W. F., Hermans, J. (1981) pp 331−342, D. Reidel Publishing Company Dordrecht, Dordrecht, Germany.
39. van Eden, W., Thole, J. E., van der Zee, R., Noordzij, A., van Embden, J. D., Hensen, E. J., and Cohen, I. R. (1988) Cloning of the mycobacterial epitope recognized by T lymphocytes in adjuvant arthritis, *Nature 331*, 171−173.
40. Adachi, T., Schamel, W. W., Kim, K. M., Watanabe, T., Becker, B., Nielsen, P. J., and Reth, M. (1996) The specificity of association of the IgD molecule with the accessory proteins BAP31/BAP29 lies in the IgD transmembrane sequence, *EMBO J. 15*, 1534−1541.
41. Quintana, F. J., Carmi, P., Mor, F., and Cohen, I. R. (2002) Inhibition of adjuvant arthritis by a DNA vaccine encoding human heat shock protein 60, *J. Immunol. 169*, 3422−3428.
42. van Eden, W., Holoshitz, J., Nevo, Z., Frenkel, A., Klajman, A., and Cohen, I. R. (1985) Arthritis induced by a T-lymphocyte clone that responds to Mycobacterium tuberculosis and to cartilage proteoglycans, *Proc. Natl. Acad. Sci. U.S.A. 82*, 5117−5120.
43. Quintana, F. J., Gerber, D., Kent, S. C., Cohen, I. R., and Shai, Y. (2005) HIV-1 fusion peptide targets the TCR and inhibits antigen-specific T cell activation, *J. Clin. Invest. 115*, 2149−2158.
44. Ali, M., De Planque, M. R. R., Huynh, N. T., Manolios, N., and Separovic, F. (2001) Biophysical studies of a transmembrane peptide derived from the T cell antigen receptor, *Lett. Pept. Sci. 8*, 227−233.
45. Reizis, B., Schild, H., Stefanovic, S., Mor, F., Rammensee, H., and Cohen, I. R. (1997) Peptide binding motifs of the MHC class I molecules (RT1.Al) of the Lewis rat, *Immunogenetics 45*, 278−279.
46. Ohashi, T., Hanabuchi, S., Suzuki, R., Kato, H., Masuda, T., and Kannagi, M. (2002) Correlation of major histocompatibility complex class I downregulation with resistance of human T-cell leukemia virus type 1-infected T cells to cytotoxic T-lymphocyte killing in a rat model, *J. Virol. 76*, 7010−7019.
47. Burrows, G. G., Ariail, K., Celnik, B., Gambee, J. E., Offner, H., and Vandenbark, A. A. (1997) Multiple class I motifs revealed by sequencing naturally processed peptides eluted from rat T cell MHC molecules, *J. Neurosci. Res. 49*, 107−116.
48. Quintana, F. J., Carmi, P., Mor, F., and Cohen, I. R. (2003) DNA fragments of the human 60-kDa heat shock protein (HSP60) vaccinate against adjuvant arthritis: identification of a regulatory HSP60 peptide, *J. Immunol. 171*, 3533−3541.
49. Call, M. E., Schnell, J. R., Xu, C., Lutz, R. A., Chou, J. J., and Wucherpfennig, K. W. (2006) The structure of the zetazeta transmembrane dimer reveals features essential for its assembly with the T cell receptor, *Cell 127*, 355−368.
50. Holoshitz, J., Matitiau, A., and Cohen, I. R. (1984) Arthritis induced in rats by cloned T lymphocytes responsive to mycobacteria but not to collagen type II, *J. Clin. Invest. 73*, 211−215.
51. Holoshitz, J., Naparstek, Y., Ben-Nun, A., and Cohen, I. R. (1983) Lines of T lymphocytes induce or vaccinate against autoimmune arthritis, *Science 219*, 56−58.
52. Anderton, S. M., van der Zee, R., Noordzij, A., and van Eden, W. (1994) Differential mycobacterial 65-kDa heat shock protein T cell epitope recognition after adjuvant arthritis-inducing or protective immunization protocols, *J. Immunol. 152*, 3656−3664.
53. Sharon, M., Oren, Z., Shai, Y., and Anglister, J. (1999) 2D-NMR and ATR-FTIR study of the structure of a cell-selective diastereomer of melittin and its orientation in phospholipids, *Biochemistry 38*, 15305−15316.
54. Oren, Z., Ramesh, J., Avrahami, D., Suryaprakash, N., Shai, Y., and Jelinek, R. (2002) Structures and mode of membrane interaction of a short alpha helical lytic peptide and its diastereomer determined by NMR, FTIR, and fluorescence spectroscopy, *Eur. J. Biochem. 269*, 3869−3880.
55. Karle, I. L., Gopi, H. N., and Balaram, P. (2003) Crystal structure of a hydrophobic 19-residue peptide helix containing three centrally located D amino acids, *Proc. Natl. Acad. Sci. U.S.A. 100*, 13946−13951.
56. Oren, Z., Hong, J., and Shai, Y. (1997) A repertoire of novel antibacterial diastereomeric peptides with selective cytolytic activity, *J. Biol. Chem. 272*, 14643−14649.
57. Papo, N., Oren, Z., Pag, U., Sahl, H. G., and Shai, Y. (2002) The consequence of sequence alteration of an amphipathic alpha-helical antimicrobial peptide and its diastereomers, *J. Biol. Chem. 277*, 33913−33921.

BI061849G